ACSNANO
www.acsnano.org
ARTICLE

Optical Gain in MoS_2 *via* Coupling with Nanostructured Substrate: Fabry–Perot Interference and Plasmonic Excitation

Hye Yun Jeong,[†,‡,#] Un Jeong Kim,[*,§,#] Hyun Kim,[†,‡] Gang Hee Han,[†,‡] Hyangsook Lee,[∥] Min Su Kim,[†,‡] Youngjo Jin,[†,‡] Thuc Hue Ly,[†,‡] Si Young Lee,[†,‡] Young-Geun Roh,[§] Won-Jae Joo,[§] Sung Woo Hwang,[§] Yeonsang Park,[*,§] and Young Hee Lee[*,†,‡]

[†]Center for Integrated Nanostructure Physics, Institute for Basic Science (IBS), Suwon 440-746, Republic of Korea
[‡]Department of Energy Science, Department of Physics, Sungkyunkwan University, Suwon 440-746, Republic of Korea
[§]Device Lab, Samsung Advanced Institute of Technology, Suwon 443-803, Republic of Korea
[∥]AE Group, Platform Technology Laboratory, Samsung Advanced Institute of Technology, Suwon 443-803, Republic of Korea

Supporting Information

ABSTRACT: **Despite the direct band gap of monolayer transition metal dichalcogenides (TMDs), their optical gain remains limited because of the poor light absorption in atomically thin, layered materials. Most approaches to improve the optical gain of TMDs mainly involve modulation of the active materials or multilayer stacking. Here, we report a method to enhance the optical absorption and emission in MoS_2 simply through the design of a nanostructured substrate. The substrate consisted of a dielectric nanofilm spacer (TiO_2) and metal film. The overall photoluminescence intensity from monolayer MoS_2 on the nanostructured substrate was engineered based on the TiO_2 thickness and amplified by Fabry–Perot interference. In addition, the neutral exciton emission was selectively amplified by plasmonic excitations from the local field originating from the surface roughness of the metal film with spacer thicknesses of less than 10 nm. We further demonstrate that the quality factor of the device can also be engineered by selecting a spacer material with a different refractive index.**

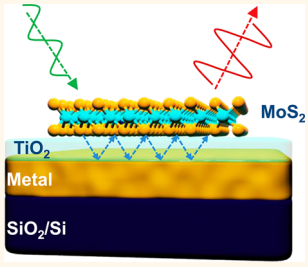

KEYWORDS: *molybdenum disulfide, photoluminescence, multireflection, Fabry–Perot interference, local field enhancement, Purcell effect*

The direct band gap of monolayer transition metal dichalcogenides (TMDs) provides great opportunities for novel optoelectronic applications such as phototransistors, solar cells, light-emitting devices (LEDs), and lasers.[1−6] Nevertheless, its low quantum efficiency (QE) inherent in atomically thin, layered materials even with large absorption coefficients has been the bottleneck in the implementation of monolayer TMDs in high-performance optoelectronic devices over other high-gain materials such as quantum dots, quantum wells, light-emitting organic materials, and direct band-gap semiconductors. Various approaches have been demonstrated to modulate the optical emission or absorption properties of TMD materials by either modification of the gain materials or substrate modulations.[7−11]

Large enhancement of the photoluminescence (PL) has been induced by p-type doping of monolayer TMD materials with TCNQ (7,7,8,8-tetracyanoquinodimethane) and O_2 physical adsorption.[7,8] Multiquantum well structures such as MoS_2/BN or polymer/MoS_2 have suggested the possibilities of cumulative enhancement by repeating the stacking of such layers.[3,9] Such multistacking techniques involve complicated device fabrication processes that cannot guarantee the stability and reliability of the chemical species, further limiting the scalability of the device integration.

Recently, optical absorption enhancement in TMD materials has been investigated under various configurations using Fabry–Perot interference *via* multireflection in layered media.[12,13] Fabry–Perot interference can be observed between two parallel reflecting interfaces with multiple internal reflections and can be extended to the optical resonance effect. The constructive resonant condition is simply tuned by changing the thickness of the spacer without any complicated structures or fabrication processes. To date, most of the works focus mainly on controlling PL intensity for single or multilayer TMD materials by optimizing the thickness of SiO_2 (spacer) formed on the semiconducting (Si) substrate in the relatively thick spacer (several hundreds of nanometers). This basic concept of Fabry–Perot interference facilitates the macroscopic

Received: May 16, 2016
Accepted: August 24, 2016
Published: August 24, 2016

DOI: 10.1021/acsnano.6b03237
ACS Nano 2016, 10, 8192–8198

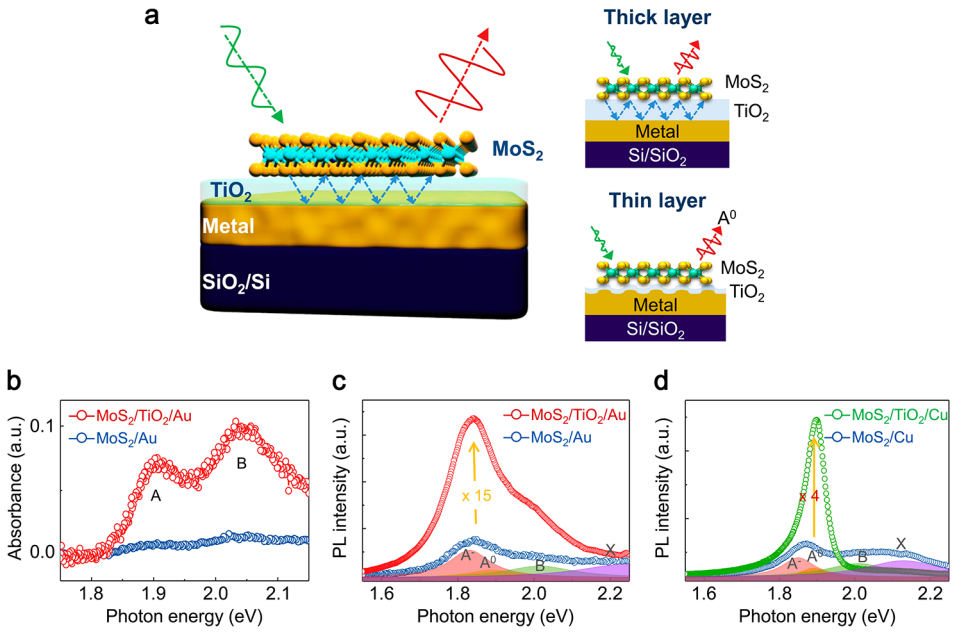

Figure 1. (a) Schematics of the PL intensity of MoS_2 on flat and corrugated metal films as a function of spacer thickness, (b) absorbance, and (c) PL spectra from different substrates measured from reflectance measurements with/without the 41 nm thick TiO_2 layer, and (d) PL spectrum of MoS_2 placed on TiO_2/Cu with/without a 3.5 nm thick TiO_2 layer.

visualization of atomically thin monolayer 2D materials, including graphene, on dielectric substrates and enables characterization of the number of layers.[12,14,15] However, there has been no significant effort to correlate this phenomenon to enhancing optical device performance.

Plasmonic nanostructures enable a boost in the generation of electron–hole pairs in 2D materials/graphene *via* local-field enhancement, resulting in increasing direct band-gap emission. All the previous works on PL enhancement[10,16,17] or photocurrent enhancement[11,18] in 2D materials/graphene have been performed by randomly spreading plasmonic metal nanoparticles on the material or patterning nanostructures using electron-beam lithography. To tune the resonance wavelength of plasmonic metal nanoparticles, completely different geometries/materials/morphologies of the metal particles need to be incorporated. Furthermore, these methods also either lack of controllability/uniformity in the device performance or involve high cost and inefficiency in the device fabrication processes.

Our aim is not to modify active TMDs because this modification alters their intrinsic optical properties, which may further degrade the sample stability. Instead, we designed the substrate to enhance the optical gain of active TMD materials. We selected the thickness of the TiO_2 spacer layer and surface roughness of the metal film as engineering parameters to enhance the optical gain of the TMD layer. We observed that the PL intensity from monolayer MoS_2 is amplified by Fabry–Perot interference, and furthermore, the local field enhancement originating from the surface roughness of the metal film becomes dominant spacer thicknesses of less than ~10 nm and selectively amplifies the neutral exciton peak. We propose that by performing analytic simulations of the transfer matrix method (TMM), the quality (Q-) factor can be engineered by selecting the spacer material to achieve a low Q-factor for broadband systems, such as solar cells and photodetectors, and a high Q-factor for complimentary image sensors with selective bands. This work provides an opportunity to optimize the performance of optoelectronic devices with various TMD materials such as LEDs, lasers, and nanoantennas.

RESULTS

Schematics of the optical coupling behavior of chemical vapor deposition (CVD)-grown monolayer MoS_2 with the nanostructured substrate are presented in Figure 1a. The incident light is partially absorbed on MoS_2 and transmitted further into the metal substrate. The reflected light at the metal substrate is again absorbed partially on MoS_2 and reflected at the MoS_2/TiO_2 interface. The repetition of absorption and reflection known as Fabry–Perot interference increases the absorption of light in MoS_2 to eventually enhance the optical gain, in particular with a thick TiO_2 layer. For a thin TiO_2 layer, the surface roughness of the metal layer generates a strong local field to enhance the light. Optical gain is attained when the spacer layer is thin enough for MoS_2 to feel the short-range local field.

Figure 1b shows the optical absorbance of monolayer MoS_2 placed on a TiO_2/Au sample. The overall absorbance was significantly increased with distinct A and B peaks near 1.9 and 2.05 eV, respectively, which is attributed to the Fabry–Perot effect. This contrasts with that without the TiO_2 spacer, where no clear A and B peaks are observed with low absorbance. Because of the enhanced absorbance, the PL intensity with the 532 nm excitation laser (3.8 mW, 0.1 s) was enhanced by 15 times while maintaining a similar PL peak shape with the neutral exciton (A^0) peak near ~1.89 eV and the B exciton peak near ~2.0 eV because of valence-band splitting due to the strong spin–orbital interaction[19,20] and multiexciton peak (~1.85 eV), mainly trion (e–h pair and one electron, A^-), which is a common feature at high laser power.[21] In contrast to this, the PL peak shape was significantly altered when a thin TiO_2 layer (3.5 nm) was deposited on the Cu film. The PL intensity was amplified by 4 times with a spacer; furthermore, the A^0 peak was selectively enhanced, whereas the other peaks were significantly diminished, as observed in Figure 1d.

DOI: 10.1021/acsnano.6b03237
ACS Nano 2016, 10, 8192–8198

The spacer thickness and metal-type dependences of the PL spectra are clearly demonstrated in Figure 2. The maximum PL

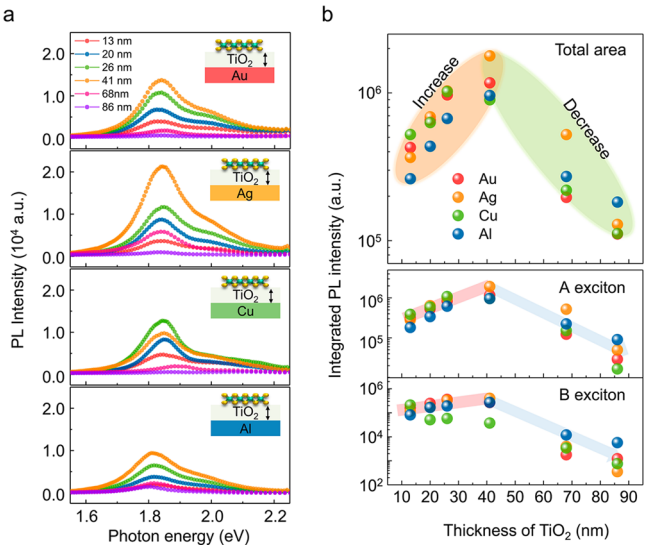

Figure 2. (a) Modification of MoS_2 PL spectral response as a function of TiO_2 thickness from 13 to 86 nm with a 532 nm excitation laser at 3.8 mW. (b) Integrated PL intensity as a function of TiO_2 thickness for various metal substrates.

intensity was clearly observed at a spacer thickness of approximately 40 nm, independent of the metal type. The intensity was altered by an order of magnitude within the spacer thickness range of 10 to 90 nm. This result is strongly correlated to the stark optical contrast at similar spacer thickness (see Supporting Information (SI), Figure S1).[14] This simply indicates that the Fabry–Perot effect plays a dominant role in enhancing the PL intensity. The peak shape was not altered with the variation in spacer thickness. The PL intensity reached a maximum for the Ag film because of its highest reflectance in the visible range among the tested metals (see SI, Figure S2).

However, the PL shape changed when the spacer thickness was less than 10 nm. In this case, the surface roughness of the metal film played an important role. To test this effect, we selected a very thin TiO_2 oxide layer ($d \approx 3.5$ nm) deposited by atomic layer deposition (ALD), and the surface roughness of Cu was modulated using different deposition conditions with a thermal evaporator.[22] The surface roughness was confirmed using cross-sectional transmission electron microscopy (TEM) images (top panel of Figure 3a). For a flat metal surface, Fabry–Perot interference remained a dominant factor in increasing the PL intensity without altering the shape, similar to the thick spacer. When the rough metal surface was introduced with a very thin oxide layer (~3.5 nm), the A^0 peak was selectively enhanced by 4.5 times compared with smooth Cu, whereas the trion and B neutral exciton peaks were significantly suppressed.

To confirm this unique selective enhancement of the PL independent of the metal type, we prepared a smooth and rough surface of an Al film with native oxide (~10 nm), again confirmed by energy-dispersive X-ray spectroscopy (EDX) mapping and TEM images (Figure 3b). To compare the roughness of the Al film further, we measured the root-mean-square (RMS) roughness using atomic force microscopy (AFM) (see SI Figure S3). Large enhancement of the A^0 peak (more than 22 times) was observed for the rough Al film compared with the smooth Al film. However, the PL enhancement was completely quenched when an additional 10 nm Al_2O_3 layer was added to the rough Al surface by ALD. The original PL shape observed on smooth Al was also recovered. The variation of the PL intensity at each step is shown in the inset of the bottom graph in Figure 3b. To guarantee selective PL enhancement, both high surface corrugation and a thin oxide layer should be used.

To investigate the effect of substrate roughness, monolayer MoS_2 was directly deposited on the smooth and rough Al surface. The deposited MoS_2 on Al does follow the general trend of roughness of the Al surface; that is, the roughness of monolayer MoS_2 (0.34 nm) on the rough substrate is higher than that (0.11 nm) on the smooth substrate, although the roughness value of MoS_2 on Al is much smaller than the Al

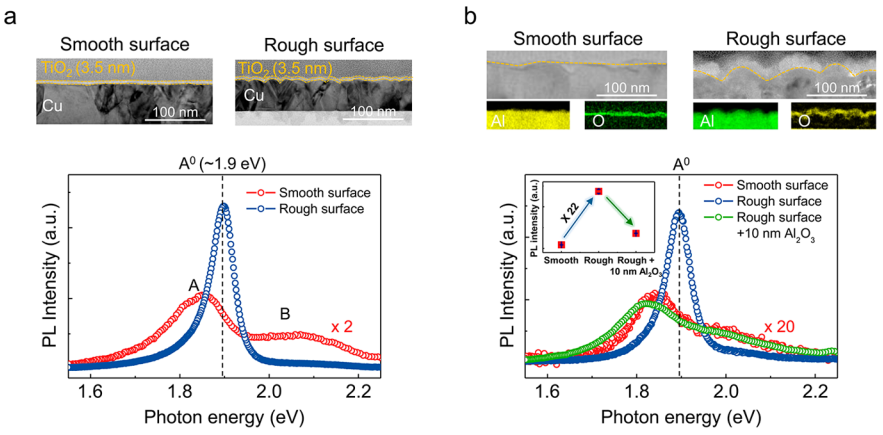

Figure 3. (a) Cross-sectional TEM images of rough and smooth Cu deposited using a thermal evaporator with different deposition conditions with a 3.5 nm thin TiO_2 film prepared by ALD. PL spectra of monolayer MoS_2 placed on the rough and smooth Cu film are shown below. (b) Cross-sectional TEM images of smooth and rough surfaces of an Al film prepared using a thermal evaporator and EDX elemental mapping images for each case (top). EDX mapping images indicate aluminum and oxygen elements. PL spectra of MoS_2 placed on a smooth (red) and rough (blue) Al surface and additional 10 nm thick Al_2O_3 film (green) on the rough Al surface. The variation of the PL intensity at each step is shown in the inset (bottom).

DOI: 10.1021/acsnano.6b03237
ACS Nano 2016, 10, 8192–8198

roughness, as shown in Figure S4, as expected. The strain on MoS_2 can be induced by the surface roughness of substrate. The strain effect on TMD materials induced by the substrate morphology has been studied by Raman spectroscopy and PL measurement. The E^1_{2g} peak of MoS_2 placed on the rough Al substrate was downshifted, which indicates that the tensile strain is applied to MoS_2 due to surface morphology. The PL intensity of MoS_2 subject to tensile strain is usually reduced, and the peak position is red-shifted in the reference.[23,24] In our case, however, the neutral PL peak intensity was exclusively enhanced, differing from the strain effect. Another possible scenario is the funnel effect that reduces the band gap and enhances PL intensity due to strain, while retaining the line shape of the PL spectrum of monolayer MoS_2.[25] This is very different from our PL spectra, again negating the possible funnel effect. Therefore, the origin of the large enhancement of the A^0 peak intensity is not from the tensile strain.

The selectively enhancement of the A^0 peak is associated with Purcell enhancement, which has been observed to be strong when the gain material is placed on a metal nanostructure.[21] The emission enhancement is due to two simultaneous processes. First, the strong local electric field on the rough surface metal nanostructure increases exciton generation in MoS_2. To investigate the field distribution around the rough metal surface, finite-difference time-domain (FDTD) calculations were conducted for the representative morphology configuration obtained from TEM images of the Cu/TiO_2 film. For the rough surface in Figure 4a, the electric

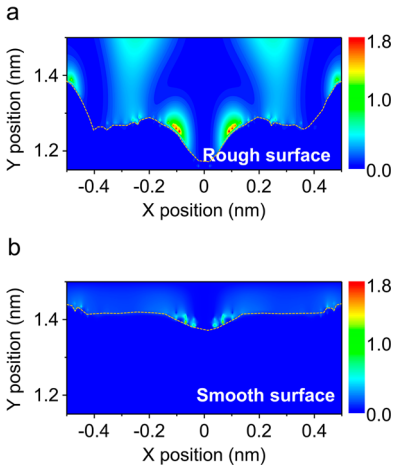

Figure 4. Electric field distribution calculated using FDTD on a (a) rough surface and (b) relatively smooth surface.

fields were strongly enhanced locally at the edges compared with the relatively smooth surface. Notably, the enhanced electric field around the valley was observed because of the localized surface plasmon effect. Second, the excitonic spontaneous emission rate of generated MoS_2 via plasmonic resonant coupling with a metal nanostructure was enhanced, as described by the Purcell effect. The nonresonant Purcell enhancement factor is defined as $F_P \equiv \Gamma_r/\Gamma_s \equiv \tau_s/\tau_r$, where Γ_r (τ_r) and Γ_s (τ_s) are the radiative decay rate (lifetime) on a rough and smooth surface in the MoS_2/spacer/metal film structure, respectively,[26]

$$\Gamma = \frac{2\pi}{\hbar}\{(d\,E(r))\}^2\rho(\omega)$$

where $E(r)$ is the electric field, $\rho(\omega)$ is the density of electromagnetic modes, and d is the electric dipole of the transition. Because $\Gamma_r > \Gamma_s$, the enhanced spontaneous emission of MoS_2 on a rough metal film restricts the formation of the trion and B peaks because of the limited band-filling effect.[21] This effect is limited to local positions within a few nanometers, as observed in Figure 4a.

In the very thin spacer regime (d < 10 nm), outstandingly selective enhancement of the A^0 peak is observed. The results in this work are critical for optical device applications. For applications that require thick oxide layers (d > 10 nm), a flat surface is more favorable because multiple reflections can be provoked more efficiently with a metal film of high reflection (see SI Figure S2). Otherwise, for optical devices, a very thin oxide layer (d < 10 nm) is necessary to avoid the PL quenching effect (see SI Figure S5), and a rough metal surface enhances the PL intensity with high selectivity of the A^0 peak. This principle can be applied to other types of TMDs.

To more clearly understand the aforementioned PL enhancement behavior by Fabry–Perot interference, simulations based on the TMM were conducted for the normal incidence of light. The reflectance, transmittance, and field profile of electromagnetic (EM) waves at the interface between layered media can be determined using the product of the matrix according to Maxwell's equations with boundary conditions at each interface. When there are multiple interfaces among adjacent layers, EM waves are partially transmitted and reflected at the interfaces. Thus, destructive or constructive interference, known as Fabry–Perot interference, can occur in layered media. In our case, two important interfaces exist: the air/TiO_2 and TiO_2/metal interfaces. As shown in Figure 5a, the SiO_2 (300 nm), metal film (100 nm), and TiO_2 layer ($0 < d <$ 100 nm) are stacked in sequence from bottom to top along the z-direction. The top surface of the TiO_2 layer is set to $z = 0$, and it is the position of the monolayer MoS_2. The material profile is presented in Figure 5b. The refractive indices of each material at 670 nm are indicated on the horizontal bottom axis. The calculated electric field intensity ($|E|^2$) is displayed on the horizontal top axis with the normal incident light of 670 nm. The resulting $|E|^2$ profiles in air are oscillatory along the z-direction. According to Fermi's golden rule, the transition probability (Γ) of electrons from the ground state to the excited state is approximately proportional to $\Gamma \approx |\vec{E}\cdot\hat{p}|^2$, where $\vec{E}$ is the electric field and $\hat{p}$ is the dipole moment of the exciton. Thus, the PL intensity from the MoS_2 layer is roughly proportional to the electric field intensity at $z = 0$ ($|E|^2(z = 0)$) where the MoS_2 layer is placed. $|E|^2(z = 0)$ is calculated as a function of the TiO_2 film thickness to determine the optimal thickness of TiO_2 for maximum PL enhancement. Figure 5b demonstrates that the electric field intensity at $z = 0$ reaches a maximum at $d \approx 41$ nm. This result is typical for Fabry–Perot interference. Constructive interference in a Fabry–Perot interferometer at the condition occurs at $2nd \cos\theta = m\lambda$, where n is the refractive index of the dielectric material between two reflecting mirrors, d is the separation of the reflecting surfaces, θ is the angle of the incident light measured from the vertical line against the reflecting surface, m is the order of interference, and λ is the wavelength of the radiation in a vacuum. In our case, $n \approx 2$ at 670 nm and $\theta = 0$, the separation difference between two consecutive constructive interferences, $\Delta d \approx \lambda/4$, which is ~167 nm. This relation can vary because one of our reflecting surfaces is metal at one side. This was confirmed from the theoretical calculations by TMM in Figure

DOI: 10.1021/acsnano.6b03237
ACS Nano 2016, 10, 8192–8198

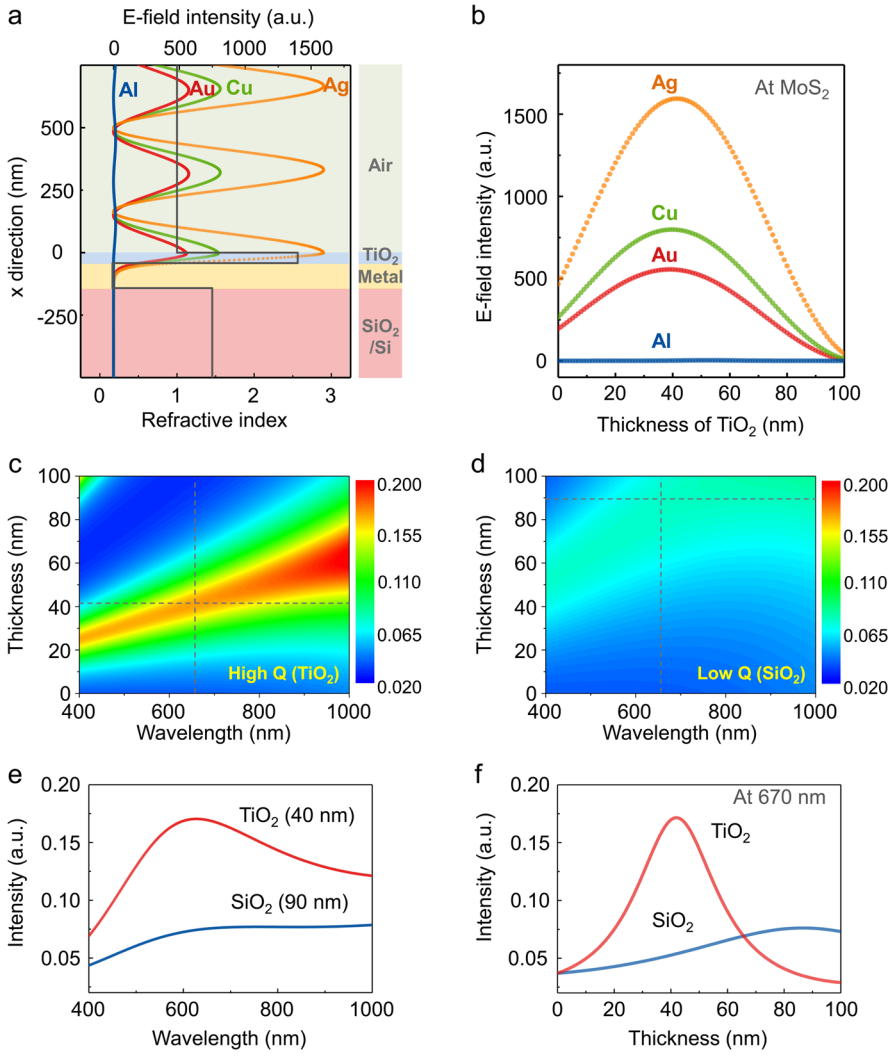

Figure 5. (a) EM field profile across the 300 nm of SiO_2, 100 nm of metal film, 41 nm of TiO_2, and air stacked in sequence. (b) EM intensity at $z = 0$ as a function of TiO_2 thickness. Electric field intensity contour maps as a function of wavelength and thickness of the spacer with (c) high refractive index material (TiO_2, 2.0) and (d) low refractive index material (SiO_2, 1.5). (e) Electric field intensity at $d = 40$ nm for high Q and $d = 90$ nm for low Q and (f) electric field intensity at 670 nm for high and low Q.

5b, $(\Delta d)/2-55$ nm, which were measured between consecutive constructive and destructive interferences.

Notably, electric field intensity increased in the order of Ag, Cu, Au, and Al, which is in reasonably good agreement with the experimental data in Figure 2b. The electric field intensity is influenced by the reflectance of metals, $R = |r^2| = \frac{|E_r^2|}{|E_i^2|}$, where R is reflectance, r is the reflectance coefficient, and E_r (E_i) is the reflected (incident) electric field. That is, a metal with strong reflectance indicates a large electric field intensity. In particular, it is remarkable that the optimal thickness with maximum field intensity, $d_{max} \approx 41$ nm, is in excellent agreement with the experimental result.

Electric field intensity contour maps as a function of the wavelength and thickness of the spacer with a low refractive index material (SiO_2) and high refractive index material (TiO_2) are presented in Figure 5c and d, respectively. TiO_2 has been utilized as the electron transport layer (ETL) in electroluminescence (EL) devices.[27,28] This result can be applied to optimize EL device performance. For example, for other gain materials emitting different wavelengths, the optimized thickness of TiO_2 should then be transformed to maximize the intensity of its luminescence.

In addition, the E-field intensity at the interface between air and the spacer depends on the thickness of the dielectric material; it is also affected by the index of the materials. Generally, a Fabry–Perot structure with a spacer of high refractive index exhibits a high quality (Q) factor, which is a dimensionless parameter that characterizes the sharpness of the resonator bandwidth. As the refractive index of the spacer increases, the reflection (R) increases. The Q-factor can be described by the equation

$$Q = \frac{2\pi d \nu_0 R}{c(1 - R^2)} \quad (1)$$

where ν_0 is the frequency, R is the reflectivity, d is the thickness of the spacer, and c is the velocity of light. The reflection at the interface between air and spacer is described as

$$R = \left| \frac{n_{spacer} - 1}{n_{spacer} + 1} \right|^2 \quad (2)$$

DOI: 10.1021/acsnano.6b03237
ACS Nano 2016, 10, 8192–8198

at normal incidence, where n_{spacer} is the refractive index of the spacer and the refractive index of air is set to be 1.

According to eqs 1 and 2, the *Q*-factor of a Fabry–Perot structure is proportional to the reflection of the two reflectors composing the structure, and thus, a structure with a high-index spacer has a higher *Q*-factor than one with a low-index spacer. Therefore, by selecting a spacer material with an appropriate index, the *Q*-factor of the structure can be simply engineered. Electric field intensity profile maps as a function of both the spacer thickness and excitation wavelength at refractive indices of n = 2.0 and 1.5 at 670 nm (which correspond to TiO_2 and SiO_2, respectively) are presented in Figure 5c and d, respectively. In Figure 5e, the electric field intensity profile reaches a maximum at 670 nm (d = 40 and 90 nm for TiO_2 and SiO_2, respectively), which is the horizontal dotted line in Figure 5c and d. Figure 5f presents the electric field intensity profile at a fixed wavelength of 670 nm, which is the vertical dotted line in Figure 5c and d. We directly compared the PL spectrum of monolayer MoS_2 deposited on TiO_2 (41 nm)/Ag substrate and SiO_2 (~90 nm)/Si substrate where PL intensities of the monolayer can be maximized according to our work and the literature.[12,14] PL from the MoS_2 deposited on TiO_2 (41 nm)/Ag substrate is measured to be ~5 times larger than that of the SiO_2/Si case (see SI Figure S6). Also, the thickness of the TiO_2 film was controlled simply by spin-coating, which is as simple as SiO_2/Si in controlling the film thickness.

For structures with low *Q*-factors, the optical responses are not selective compared with high-*Q* devices. Thus, these structures may be suitable for broadband photoresponsive devices such as solar cells and broadband photodetectors. Otherwise, high-*Q* structures with high-index materials can be applied for selective band response devices such as R-, G-, and B-image sensors.

CONCLUSION

We have systematically studied the modulation of the PL intensity from monolayer MoS_2 placed on TiO_2/metals (Au, Ag, Cu, and Al) as a function of the TiO_2 thickness and surface morphology of the metal. The PL intensity from monolayer MoS_2 was generally governed by Fabry–Perot interference; in addition, field enhancement of the optical emission originating from the surface roughness of the metal film was observed to become dominant for thin spacers (<~10 nm). A TiO_2 thickness of 41 nm at 670 nm was the optimized value to achieve the highest PL intensity of MoS_2, which was remarkably consistent with analytical calculations performed using the TMM. Depending on the wavelength of our interest, the optimized thickness of the spacer and metal material can be engineered. Notably, the A^0 peak was selectively enhanced by ~22 times for an Al substrate with a rough surface, which is differentiated from the PL spectrum profile (maintaining the ratio of A and B excitons) for thick spacers (>~10 nm). By designing the material of the spacer, we have conceptually demonstrated that the *Q*-factor of the device can be engineered depending on the target device application (for broadband or highly selective band applications). This work is broadly applicable to optimize the TMD material incorporated in optical devices such as LEDs, lasers, and plasmonic hybrid devices (*e.g.*, nanoantennas).

METHODS

Substrate Preparation. The Au, Ag, Cu, and Al (~50 nm) films were deposited using a thermal evaporator on SiO_2 (300 nm)/Si substrates. The surface roughness of the Cu and Al films was controlled by deposition conditions such as the deposition rate and distance between the source target and substrate. The thin TiO_2 layer was deposited on the Au, Ag, Cu, and Al/SiO_2/Si substrates using two methods. The thin TiO_2 layer of less than 10 nm was deposited by ALD at 200 °C with titanium isopropoxide as a source and deionized (DI) water as an oxidation agent. The thick TiO_2 layer (titanium(IV) butoxide solution, 5 wt % in *n*-butanol) of more than 10 nm was spin-coated (2000 rpm, 60 s) onto the metal film/SiO_2/Si substrate. The thickness of the TiO_2 layer was controlled by the ratio of *n*-butanol to a 5 wt % TiO_2 solution (see SI Figure S7). The TiO_2/metal film/SiO_2/Si substrates were annealed at 100 °C for 15 min in air.

Growth of Monolayer MoS_2. An ammonium heptamolybdate (AHM, Sigma-Aldrich, 431346) powder was used as a Mo precursor. The AHM was dissolved in DI water. The solution (6 μL) was dropped onto a quartz wafer (2 mm × 20 mm). The Mo precursor quartz wafer was placed inside a dry oven (~80 °C). The Mo precursor quartz wafer was placed next to the target wafer, which was coated by a sodium cholate solution in the reactor. The sulfur (S) source (200 mg) was placed far away from the Mo precursor quartz wafer and target wafer. The Mo heating zone was heated to 780 °C at a ramping rate of 78 °C/min, and the temperature of the S zone was ramped up to 210 °C (42 °C/min). During the entire process, N_2 (500 sccm) was injected as a carrier gas.

Sample Preparation. The CVD-grown monolayer MoS_2 was transferred onto a TiO_2/metal film/SiO_2/Si substrate with a poly(methyl methacrylate) (PMMA) support. The PMMA A4 (Micro Chem, 4 wt % in anisole) was spin-coated onto the as-grown MoS_2/SiO_2/Si at 1500 rpm for 60 s. To detach the MoS_2/PMMA film from the SiO_2/Si substrate, the PMMA/MoS_2/SiO_2/Si substrate was placed into a hot 1 M potassium hydroxide (KOH) solution for a few minutes, and then, the PMMA/MoS_2 layer was floated onto the KOH solution. Next, the PMMA/MoS_2 was rinsed four times using DI water. Finally, the PMMA/MoS_2 layer was picked up by the prepared substrate and then dried in air. The PMMA was removed using acetone, and the sample was rinsed with isopropyl alcohol.

Characterization. The morphology of the CVD-grown MoS_2 on TiO_2/Au film/SiO_2/Si substrate was examined using optical microscopy (100× magnification, WEISS, Axio Imager 2). Confocal microPL measurements were performed using commercial equipment (NTEGRA spectra, PNL NT MDT) with an exciting laser wavelength of 532 nm and a 100× objective (NA = 0.7) lens. The reflectance of the metals was measured using a commercial spectrophotometer (V-670, JASCO). The thickness of the TiO_2 layer was observed using TEM (FEI OSIRIS). The roughness of each metal (Au, Ag, Cu, and Al) was observed using AFM (Nano Navi) in contact mode (see SI Figures S3 and S8). All of them exhibited subnanometer RMS roughness.

ASSOCIATED CONTENT

Supporting Information

The Supporting Information is available free of charge on the ACS Publications website at DOI: 10.1021/acsnano.6b03237.

Supporting Figures S1–S8 (PDF)

AUTHOR INFORMATION

Corresponding Authors

*E-mail: ujjane.kim@samsung.com.
*E-mail: yeonsang.park@samsung.com.
*E-mail: leeyoung@skku.edu.

Author Contributions

#H. Y. Jeong and U. J. Kim contributed equally to this work.

Notes

The authors declare no competing financial interest.

DOI: 10.1021/acsnano.6b03237
ACS Nano 2016, 10, 8192–8198

ACKNOWLEDGMENTS

This work was supported by IBS-R011-D1 and the Human Resources Development Program (No. 20124010203270) of a Korea Institute of Energy Technology Evaluation and Planning (KETEP) grant funded by the Korean government Ministry of Trade, Industry, and Energy.

REFERENCES

(1) Lopez-Sanchez, O.; Lembke, D.; Kayci, M.; Radenovic, A.; Kis, A. Ultrasensitive Photodetectors Based on Monolayer MoS_2. *Nat. Nanotechnol.* **2013**, *8*, 497−501.

(2) Yin, Z. Y.; Li, H.; Li, H.; Jiang, L.; Shi, Y. M.; Sun, Y. H.; Lu, G.; Zhang, Q.; Chen, X. D.; Zhang, H. Single-Layer MoS_2 Phototransistors. *ACS Nano* **2012**, *6*, 74−80.

(3) Withers, F.; Del Pozo-Zamudio, O.; Mishchenko, A.; Rooney, A. P.; Gholinia, A.; Watanabe, K.; Taniguchi, T.; Haigh, S. J.; Geim, A. K.; Tartakovskii, A. I.; Novoselov, K. S. Light-Emitting Diodes by Band-Structure Engineering in van der Waals Heterostructures. *Nat. Mater.* **2015**, *14*, 301−306.

(4) Li, D. H.; Cheng, R.; Zhou, H. L.; Wang, C.; Yin, A. X.; Chen, Y.; Weiss, N. O.; Huang, Y.; Duan, X. F. Electric-Field-Induced Strong Enhancement of Electroluminescence in Multilayer Molybdenum Disulfide. *Nat. Commun.* **2015**, *6*, 7509.

(5) Tsai, M. L.; Su, S. H.; Chang, J. K.; Tsai, D. S.; Chen, C. H.; Wu, C. I.; Li, L. J.; Chen, L. J.; He, J. H. Monolayer MoS_2 Heterojunction Solar Cells. *ACS Nano* **2014**, *8*, 8317−8322.

(6) Wu, S. F.; Buckley, S.; Schaibley, J. R.; Feng, L. F.; Yan, J. Q.; Mandrus, D. G.; Hatami, F.; Yao, W.; Vuckovic, J.; Majumdar, A.; Xu, X. D. Monolayer Semiconductor Nanocavity Lasers with Ultralow Thresholds. *Nature* **2015**, *520*, 69−76.

(7) Nan, H. Y.; Wang, Z. L.; Wang, W. H.; Liang, Z.; Lu, Y.; Chen, Q.; He, D. W.; Tan, P. H.; Miao, F.; Wang, X. R.; Wang, J. L.; Ni, Z. H. Strong Photoluminescence Enhancement of MoS_2 through Defect Engineering and Oxygen Bonding. *ACS Nano* **2014**, *8*, 5738−5745.

(8) Mouri, S.; Miyauchi, Y.; Matsuda, K. Tunable Photoluminescence of Monolayer MoS_2 *via* Chemical Doping. *Nano Lett.* **2013**, *13*, 5944−5948.

(9) Joo, P.; Jo, K.; Ahn, G.; Voiry, D.; Jeong, H. Y.; Ryu, S.; Chhowalla, M.; Kim, B. S. Functional Polyelectrolyte Nanospaced MoS_2 Multi layers for Enhanced Photoluminescence. *Nano Lett.* **2014**, *14*, 6456−6462.

(10) Butun, S.; Tongay, S.; Aydin, K. Enhanced Light Emission from Large-Area Monolayer MoS_2 Using Plasmonic Nanodisc Arrays. *Nano Lett.* **2015**, *15*, 2700−2704.

(11) Sobhani, A.; Lauchner, A.; Najmaei, S.; Ayala-Orozco, C.; Wen, F. F.; Lou, J.; Halas, N. J. Enhancing the Photocurrent and Photoluminescence of Single Crystal Monolayer MoS_2 with Resonant Plasmonic Nanoshells. *Appl. Phys. Lett.* **2014**, *104*, 031112.

(12) Lien, D. H.; Kang, J. S.; Amani, M.; Chen, K.; Tosun, M.; Wang, H. P.; Roy, T.; Eggleston, M. S.; Wu, M. C.; Dubey, M.; Lee, S. C.; He, J. H.; Javey, A. Engineering Light Outcoupling in 2D Materials. *Nano Lett.* **2015**, *15*, 1356−1361.

(13) Liu, J. T.; Wang, T. B.; Li, X. J.; Liu, N. H. Enhanced Absorption of Monolayer MoS_2 with Resonant Back Reflector. *J. Appl. Phys.* **2014**, *115*, 193511.

(14) Wang, Y. Y.; Ni, Z. H.; Shen, Z. X.; Wang, H. M.; Wu, Y. H. Interference Enhancement of Raman Signal of Graphene. *Appl. Phys. Lett.* **2008**, *92*, 043121.

(15) Han, G. H.; Chae, S. J.; Kim, E. S.; Gunes, F.; Lee, I. H.; Lee, S. W.; Lee, S. Y.; Lim, S. C.; Jeong, H. K.; Jeong, M. S.; Lee, Y. H. Laser Thinning for Monolayer Graphene Formation: Heat Sink and Interference Effect. *ACS Nano* **2011**, *5*, 263−268.

(16) Najmaei, S.; Mlayah, A.; Arbouet, A.; Girard, C.; Leotin, J.; Lou, J. Plasmonic Pumping of Excitonic Photoluminescence in Hybrid MoS_2-Au Nanostructures. *ACS Nano* **2014**, *8*, 12682−12689.

(17) Gao, W.; Lee, Y. H.; Jiang, R. B.; Wang, J. F.; Liu, T. X.; Ling, X. Y. Localized and Continuous Tuning of Monolayer MoS_2 Photoluminescence Using a Single Shape-Controlled Ag Nanoantenna. *Adv. Mater.* **2016**, *28*, 701−706.

(18) Lin, J. D.; Li, H.; Zhang, H.; Chen, W. Plasmonic Enhancement of Photocurrent in MoS_2 Field-Effect-Transistor. *Appl. Phys. Lett.* **2013**, *102*, 203109.

(19) Splendiani, A.; Sun, L.; Zhang, Y. B.; Li, T. S.; Kim, J.; Chim, C. Y.; Galli, G.; Wang, F. Emerging Photoluminescence in Monolayer MoS_2. *Nano Lett.* **2010**, *10*, 1271−1275.

(20) Eda, G.; Yamaguchi, H.; Voiry, D.; Fujita, T.; Chen, M. W.; Chhowalla, M. Photoluminescence from Chemically Exfoliated MoS_2. *Nano Lett.* **2011**, *11*, 5111−5116.

(21) Lee, H. S.; Kim, M. S.; Jin, Y.; Han, G. H.; Lee, Y. H.; Kim, J. Selective Amplification of the Primary Exciton in a MoS_2 Monolayer. *Phys. Rev. Lett.* **2015**, *115*, 226801.

(22) Bordo, K.; Rubahn, H. G. Effect of Deposition Rate on Structure and Surface Morphology of Thin Evaporated Al Films on Dielectrics and Semiconductors. *Mater. Sci. Medzg.* **2012**, *18*, 313−317.

(23) Conley, H. J.; Wang, B.; Ziegler, J. I.; Haglund, R. F.; Pantelides, S. T.; Bolotin, K. I. Bandgap Engineering of Strained Monolayer and Bilayer MoS_2. *Nano Lett.* **2013**, *13*, 3626−3630.

(24) Liu, Z.; Amani, M.; Najmaei, S.; Xu, Q.; Zou, X. L.; Zhou, W.; Yu, T.; Qiu, C. Y.; Birdwell, A. G.; Crowne, F. J.; Vajtai, R.; Yakobson, B. I.; Xia, Z. H.; Dubey, M.; Ajayan, P. M.; Lou, J. Strain and Structure Heterogeneity in MoS_2 Atomic Layers Grown by Chemical Vapour Deposition. *Nat. Commun.* **2014**, *5*, 5246.

(25) Li, H.; Contryman, A. W.; Qian, X. F.; Ardakani, S. M.; Gong, Y. J.; Wang, X. L.; Weisse, J. M.; Lee, C. H.; Zhao, J. H.; Ajayan, P. M.; Li, J.; Manoharan, H. C.; Zheng, X. L. Optoelectronic Crystal of Artificial Atoms in Strain-Textured Molybdenum Disulphide. *Nat. Commun.* **2015**, *6*, 7381.

(26) Boroditsky, M.; Vrijen, R.; Krauss, T. F.; Coccioli, R.; Bhat, R.; Yablonovitch, E. Spontaneous Emission Extraction and Purcell Enhancement from Thin-Film 2-D Photonic Crystals. *J. Lightwave Technol.* **1999**, *17*, 2096−2112.

(27) Cho, K. S.; Lee, E. K.; Joo, W. J.; Jang, E.; Kim, T. H.; Lee, S. J.; Kwon, S. J.; Han, J. Y.; Kim, B. K.; Choi, B. L.; Kim, J. M. High-Performance Crosslinked Colloidal Quantum-Dot Light-Emitting Diodes. *Nat. Photonics* **2009**, *3*, 341−345.

(28) Sadhanala, A.; Kumar, A.; Pathak, S.; Rao, A.; Steiner, U.; Greenham, N. C.; Snaith, H. J.; Friend, R. H. Electroluminescence from Organometallic Lead Halide Perovskite-Conjugated Polymer Diodes. *Adv. Electron. Mater.* **2015**, *1*, 1500008.

DOI: 10.1021/acsnano.6b03237
ACS Nano 2016, 10, 8192−8198